GEOPHYSICAL RESEARCH LETTERS, VOL. 27, NO. 22, PAGES 3675-3678, NOVEMBER 15, 2000

An empirical model of the ionospheric electric potential

A. J. Ridley[1], G. Crowley[2], C. Freitas[2]

Abstract.
We present an empirical model of the ionospheric electric potential based on output from the assimilative mapping of ionospheric electrodynamics technique (AMIE). The model is derived using a multivariable linear regression analysis technique to relate the potential at each grid point to the interplanetary magnetic field B_y and B_z components. AMIE output over a one week period was used to construct the model. The results of the model are very similar to other electric potential models; namely, the background pattern and the model response to B_y and B_z are typical. The unique aspect of this model is the use of the linear response to changes in IMF for the forward prediction of the potential pattern. We show an example of how the model can significantly improve predictions of the potential when it is coupled to a real-time specification model such as the real-time version of AMIE.

Introduction

There exist many models which describe the ionospheric electric field structure, most of which provide only a few electric potential patterns for selected IMF and solar wind conditions. For example, the *Heppner and Maynard* [1987] model is based upon electric field measurements made by Dynamics Explorer 2 (DE-2) and provides seven convection patterns for different IMF orientations. Other models, which incorporate both more IMF orientations and seasonal effects, are those presented by *Rich and Hairston* [1994], *Weimer* [1995], and *Ruohoniemi and Greenwald* [1996]. These three models each offer approximately 75 different electric field patterns for a wide variety of fixed IMF orientations and seasons. The above models agree on the basic structure of the ionospheric convection: for example, the antisunward flow over the magnetic pole when the IMF B_z is southward.

Another type of statistical model is one that allows the electric field pattern to be modeled for any IMF orientation. This type of model is more versatile than the above mentioned models by allowing small changes in IMF orientation to be reflected in the electric field structure [*Friis-Christensen et al.*, 1985; *Papitashvili et al.*, 1994; *Weimer*, 1996]. These models accomplish this by either fitting spherical harmonic coefficients to functions [*Weimer*, 1996], or having a physical assumption about the linearity of the system [*Friis-Christensen et al.*, 1985; *Papitashvili et al.*, 1994].

In this letter we present an empirical model of the northern hemisphere electric potential pattern based on output from the assimilative mapping of ionospheric electrodynamics (AMIE) technique [*Richmond and Kamide*, 1988]. This model is an empirical model of the potential based on the measured upstream IMF orientation, and is similar in nature to the models presented by *Papitashvili et al.* [1994] and *Friis-Christensen et al.* [1985]. The main purpose of this model is to predict the future ionospheric electrodynamic state when given the current current ionospheric state (as determined by AMIE), and the upstream IMF conditions.

Technique

Papitashvili et al. [1994] and *Friis-Christensen et al.* [1985] reported on the relationship between ground based magnetic perturbations and IMF B_y and B_z. Once these relationships were determined, potential patterns were derived using the magnetic perturbations and a static conduc-

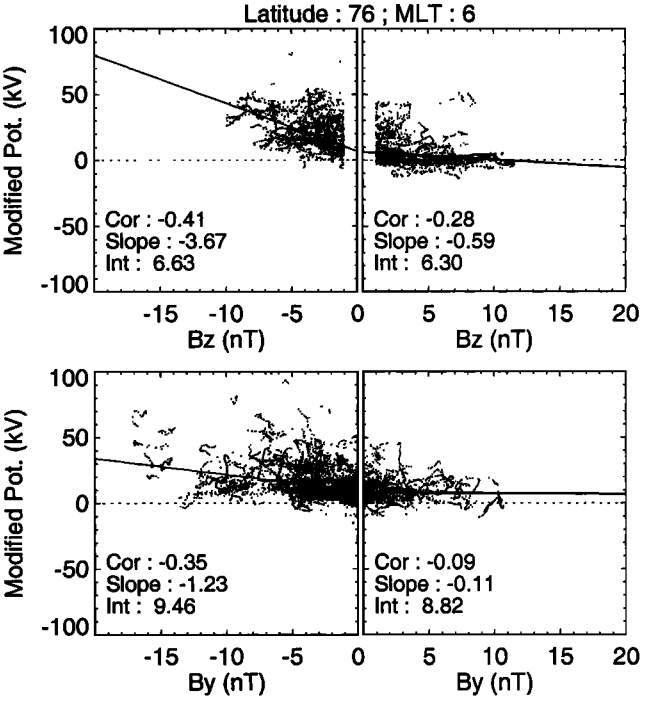

Figure 1. The relationship between the AMIE derived electric potential at 76° latitude, 06 MLT, and B_z (top) and B_y (bottom). Negative (left) and positive (right) value of the different components are separated for the fits. The cross correlation coefficient (Cor:), Slope, and y-intercept (Int:) are specified in each plot.

[1]The University of Michigan, Ann Arbor.
[2]Southwest Research Institute, San Antonio, Texas.

Copyright 2000 by the American Geophysical Union.

Paper number 1999GL011161
0094-8276/00/1999GL011161$05.00

tance model. The Statistical AMIE model (SAMIE) was derived using a linear regression analysis technique, similar to that used by *Papitashvili et al.* [1994] and *Friis-Christensen et al.* [1985]. With the model presented here, individual electric potential patterns were derived using approximately 100 ground magnetometer stations. Background conductance patterns based on the hemispheric power index measured by NOAA and DMSP satellites [*Fuller-Rowell and Evans*, 1987] were altered by AMIE using the magnetometer data as specified by *Ahn et al.* [1983].

For this initial version of SAMIE, 1 minute AMIE runs were used from March 23 thru March 30, 1995. The IMF was measured by the WIND satellite upstream of the magnetosphere. The measured values were convected to the dayside magnetopause using the distance of the satellite away from the subsolar magnetopause along the Sun-Earth direction and the measured solar wind bulk speed. An additional 10 minutes were added to account for the slow convection through the magnetosheath and the magnetopause-ionosphere communication time [*Ridley et al.*, 1998]. For the linear regression analysis, the convected IMF data was smoothed using a 15 minute running average, while the AMIE patterns were smoothed in time using a 5 minute running average. The individual AMIE patterns were not smoothed in latitude or longitude.

Figure 1 shows a plot of the AMIE-derived electric potential at 76° magnetic latitude and 06 MLT versus the IMF Z and Y components. We have separated each component into positive and negative values for two reasons: (1) it is expected that currents will flow in different regions for B_z negative and positive, which causes the linearity in the potential for negative and positive B_z to be different; and (2) the linear fits are better when B_y is separated into negative and positive values.

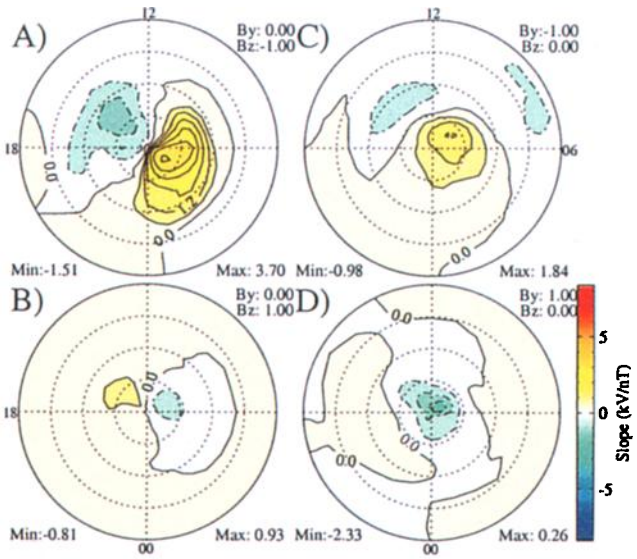

Plate 1. A map of the electric potential added to the background potential for (A) $B_z = -1.0nT$, (B) $B_z = +1.0nT$, (C) $B_y = -1.0$, (D) $B_y = +1.0$. These plots are in magnetic latitude versus magnetic local time coordinates, with the magnetic pole at the center and 50° at the outer boundary. The top of each plot represents noon, while the right side is dawn.

At this location (i.e. near the morning convection reversal boundary), B_z is the dominant component, establishing both the strength and location of the morning maximum in potential. Figure 1 shows this to be the case, with the potential increasing significantly with increasingly negative B_z. The potential shows little to no relationship with B_y. Using a multivariable linear regression analysis, it is determined that at this location, the potential is given as:

$$\Psi_{B_z-} = 3.67|B_z| + 3.90kV \quad (1)$$

$$\Psi_{B_z+} = -0.59B_z + 3.90kV \quad (2)$$

$$\Psi_{B_y-} = 1.23|B_y| + 3.90kV \quad (3)$$

$$\Psi_{B_y+} = -0.11B_y + 3.90kV \quad (4)$$

for the different components of the IMF. The total electric potential is the sum of the B_y and B_z related potentials. For example, if B_y is -1.0 nT, and B_z is 4.0 nT, $\Psi = \Psi_{B_z+} + \Psi_{B_y-}$, so that $\Psi = 1.54kV + 5.13kV = 6.67kV$.

The linear regression analysis was carried out at every point on the AMIE grid (i.e. 2° latitude down to 46° by 1 hour MLT). The analysis gave grids of slopes and intercepts for B_y and B_z negative and positive. Each map has been smoothed by averaging each data point with its four nearest neighbors. Each point is weighted using the cross correlation coefficient of the potential and the respective IMF component for that location, with the central point having a weighting of four times it's cross correlation coefficient. The pole is given as the average of all of the 88° grid points. It is expected that the maps of the intercepts for all four combinations of B_y and B_z negative and positive should be relatively similar, since they are all IMF independent potential patterns (i.e. the statistical average viscous interaction potential pattern). We have averaged all of these background patterns together to form a single background pattern (hence the same intercept for Equations 1-4, which is the viscous potential divided by two for both the B_y and B_z component). This background pattern is very similar to other estimates of the viscous interaction potential [*Reiff and Burch*, 1985; *Papitashvili et al.*, 1994], and has a cross polar potential of approximately 18 kV.

Plate 1 displays the slopes multiplied by unit vectors for the different linear fits. The top map (A) shows the relationship between the electric potential and negative B_z. This is a two cell convection pattern for which magnetic flux is being moved antisunward over the pole. Each cell is approximately equal in spatial size, with the morning cell being approximately twice the strength of the afternoon cell. The second map (B) shows the relationship when B_z is positive. This map is quite different than the B_z negative map, as expected. In this case there are still two distinct cells, but they are of opposite polarity and much smaller both spatially and in magnitude than the previous case. This implies that when B_z is positive, the magnetic flux is convected sun-

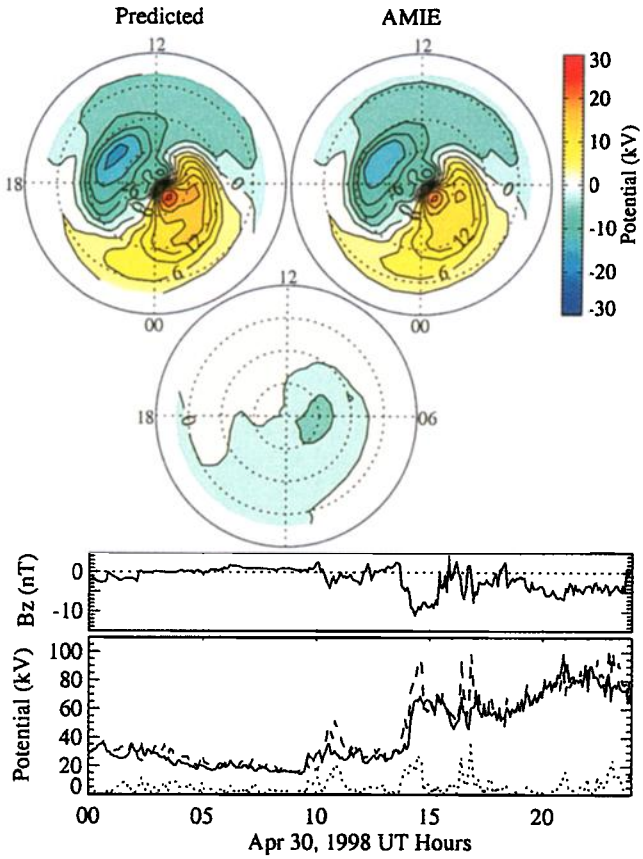

Plate 2. Plots of the SAMIE predicted (upper left) and the AMIE derived (upper right) ionospheric potential in the same format as the plots in Figure 1. These are 24 hour averages of 5 minute runs on April 30, 1998. The central circular plot is the difference between the two. The top temporal plot is the IMF B_z, while the bottom plot shows the AMIE (solid) and SAMIE (dashed) derived cross polar cap potential and the difference between the two (dotted).

ward at high latitudes, as is commonly agreed upon. The last two maps (C and D) show single cells centered near the pole, and of opposite polarity for B_y negative (C) and positive (D). These single cell patterns show that B_y controls the east-west direction of the flow near the cusp, with B_y negative (positive) causing eastward (westward) flow in the cusp region. These patterns are very similar to those reported by *Crowley et al.* [1992], *Papitashvili et al.* [1994], and *Ridley et al.* [1998].

Discussion and Conclusions

The model described above is quite useful in a number of ways. For example, as a stand alone model it can predict the electric potential given the upstream solar wind and IMF conditions in a similar manner as can be done with other electric potential models [e.g. *Weimer*, 1996; *Papitashvili et al.*, 1994; *Ruohoniemi and Greenwald*, 1996]. It can also be combined with ground and satellite-based data to produce improved predictions using a real-time version of AMIE. The current state of the ionosphere is specified using all of the available ground and satellite based measurements. Once this has been done, the upstream IMF conditions (with an approximately one hour lag time) can be used to drive SAMIE. This is done by taking the difference between the IMF at the time of the AMIE specified pattern and the future IMF, applying the differences in B_y and B_z to the slope maps shown in Plate 1, then adding the derived pattern to the AMIE specified electric potential pattern. This produces an arguably more accurate prediction of the electric potential pattern, given real-time ground based data, satellite data, and the upstream solar wind and IMF conditions.

We present an example of the predictive capabilities in Plate 2, which shows a comparison of the SAMIE one hour forward prediction values of the potential (averaged over 24 hours), the AMIE derived values of the potential (averaged over the same period), and the difference between them. The bottom plots show the time shifted IMF B_z component and the cross polar cap potential as a time series. During this period, B_z was northward for almost half the time. The averaged AMIE plots indicate that there was reversed convection during this time period. The 24-hour averages are very similar, with the strongest difference being on the night side and in the dawn sector.

The time series plots show how AMIE and SAMIE can interact to give the best prediction possible. For example, at 1400 UT, B_z becomes strongly negative, so the prediction

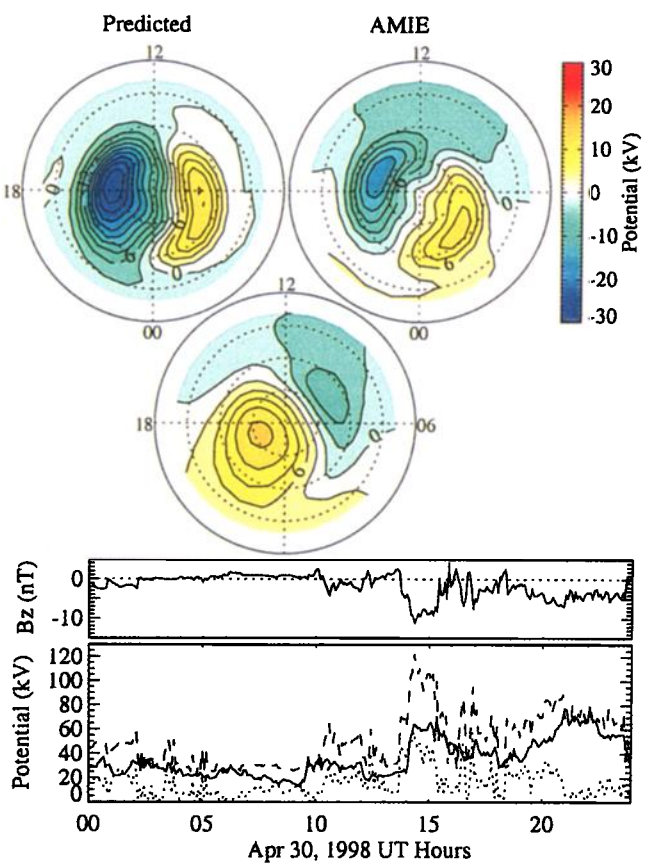

Plate 3. A comparison of the *Weimer* [1996] and the AMIE derived potential in the same format as Figure 2.

shows the potential to be very large compared to the actual potential. Once the predictive model starts using the AMIE patterns after the IMF reorientation, though, the potentials equal out and the difference is minimized. This drives the predicted values back towards the ground and satellite based measurements, which allows some decoupling from the IMF measurements made by the upstream satellite.

We compare the coupled model run to a non-interactive background model run. Plate 3 shows the 24 hour average *Weimer* [1996] pattern, the AMIE pattern using that background, and the difference between them. This run was conducted using the same data sets as the previous run, but with a different background model selected. The AMIE potential pattern (right) is much weaker than the *Weimer* [1996] patterns (left), and there is very little hint of the reversed convection, which was clearly observed in the previous run. Comparing Plates 2 and 3, it is evident that AMIE heavily relies on the background pattern for data sparse regions (e.g. the central polar cap). It is also evident that there are significant differences between AMIE and *Weimer* [1996].

The time series plot in Plates 3 shows that by having a non-interactive model, such as *Weimer* [1996], as a background pattern, there can be no correction to the predicted potential pattern. If the potential is overestimated at one time and the IMF is steady, the prediction will be overestimated for all times.

While the SAMIE model as presented in this letter is an adequate first step, a number of improvements could be made: (1) the southern hemisphere could be included; (2) more time periods, covering all seasons, could be included to elucidate asymmetries between the strength and shape of the electric potential during different seasons; (3) the electric field could be used in regions of low potential so that the cross correlation may improve in those regions; (4) the B_z positive to negative split could be moved closer to 2 nT, as indicated by *Braugitam et al.* [1991]; and (5) a more sophisticated relationship could be established between the nightside electric field or potential and the upstream IMF and solar wind conditions (e.g. using a time series of IMF data combined with a linear filter).

Acknowledgments. This research was supported at Southwest Research Institute by an internal research grant and from NSF by grants ATM-9802149 and ATM-0077555. Data used in AMIE were provided by: the Canadian Space Agency, the Danish meteorological institute, the IMAGE project, the University of Leicester (SAMNET), K. Yumoto at Kyushu University (210MM), USGS, NGDC, NASA (WIND MFI), MIT (WIND SWE), NOAA (HPI), and AFRL (HPI).

References

Ahn, B.-H., R.M. Robinson, Y. Kamide, and S.-I. Akasofu, Electric conductivities, electric fields and auroral particle energy injection rate in the auroral ionosphere and their empirical relations to horizontal magnetic disturbances, *Planet. Space Sci.*, *31*, 641, 1983.

Braugitam, D.H., M.S. Gussenhoven, and D.A. Hardy, A statistical study on the effects of IMF B_z and solar wind speed on auroral ion and electron precipitation, *J. Geophys. Res.*, *96*, 5525, 1991.

Crowley, G., P.S. Cannon, C.G. Dozois, B.W. Reinisch, and J. Buchau, Polar cap convection for B_z northward, *Geophys. Res. Lett.*, *19*, 657, 1992.

Friis-Christensen, E., Y. Kamide, A.D. Richmond, and S. Matsushita, Interplanetary magnetic field control of high-latitude electric fields and currents determined from Greenland magnetometer chain, *J. Geophys. Res.*, *90*, 1325, 1985.

Fuller-Rowell, T.J., and D.S. Evans, Height-integrated Pedersen and Hall conductivity patterns inferred from TIROS–NOAA satellite data, *J. Geophys. Res.*, *92*, 7606, 1987.

Heppner, J.P., and N.C. Maynard, Empirical high-latitude electric field models, *J. Geophys. Res.*, *92*, 4467, 1987.

Papitashvili, V.O., B.A. Belov, D.S. Faermark, Y.I. Feldstein, S.A. Golyshev, L.I. Gromova, and A.E. Levitin, Electric potential patterns in the northern and southern polar regions parameterized by the interplanetary magnatic field, *J. Geophys. Res.*, *99*, 13,251, 1994.

Reiff, P.H., and J.L. Burch, IMF B_y-dependent plasma flow and Birkeland currents in the dayside magnetopause, 2, A global model for nothward and southward IMF, *J. Geophys. Res.*, *90*, 1595, 1985.

Rich, F.J., and M. Hairston, Large-scale convection patterns observed by DMSP, *J. Geophys. Res.*, *99*, 3827, 1994.

Richmond, A.D., and Y. Kamide, Mapping electrodynamic features of the high-latitude ionosphere from localized observations: Technique, *J. Geophys. Res.*, *93*, 5741, 1988.

Ridley, A.J., C.R. Clauer, G. Lu, and V.O. Papitashvili, A statistical study of the ionospheric convection response to changing interplanetary magnetic field conditions using the assimilative mapping of ionospheric electrodynamics technique, *J. Geophys. Res.*, *103*, 4023, 1998.

Ruohoniemi, J.M., and R.A. Greenwald, Statistical patterns of the high-latitude convection obtained from Goose Bay HF radar observations, *J. Geophys. Res.*, *101*, 21,743, 1996.

Weimer, D.R., Models of high-latitude electric potentials derived with a least error fit of spherical harmonic coefficients, *J. Geophys. Res.*, *100*, 19,595, 1995.

Weimer, D.R., A flexible, IMF dependent model of high-latitude electric potential having "space weather" applications, *Geophys. Res. Lett.*, *23*, 2549, 1996.

A. J. Ridley, 1411B Space Research Building, The University of Michigan, Ann Arbor, MI 48109-2143. (e-mail: ridley@umich.edu)

G. Crowley, C. Freitas, Southwest Research Institute, 6220 Culebra Road, San Antonio, TX 78238-5166. (e-mail: ridley@umich.edu)

(Received October 19, 1999; revised February 3, 2000; accepted June 13, 2000.)